IEEE Photonics Journal
An IEEE Photonics Society Publication

Open Access

Tunable Plasmon-Induced Transparency in Dual Hexagonal Resonators With Rotatable Embedded Bar

Volume 11, Number 6, December 2019

Yichen Ye
Yiyuan Xie
Tingting Song
Bocheng Liu
Junxiong Chai
Liangyi Zhang
Yunchao Zhu
Yong Liu

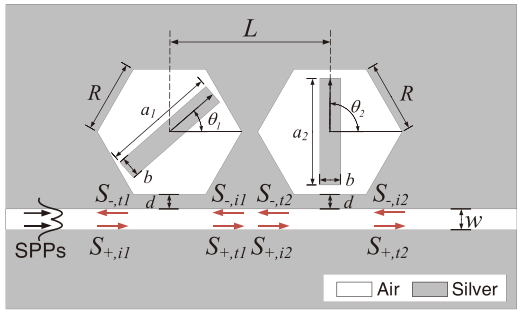

DOI: 10.1109/JPHOT.2019.2945395

Tunable Plasmon-Induced Transparency in Dual Hexagonal Resonators With Rotatable Embedded Bar

Yichen Ye,[1] Yiyuan Xie ,[1,2,3] Tingting Song,[1] Bocheng Liu,[1] Junxiong Chai,[1] Liangyi Zhang,[1] Yunchao Zhu,[1] and Yong Liu[3]

[1]College of Electronic and Information Engineering, Southwest University, Chongqing 400715, China
[2]Chongqing Key Laboratory of Nonlinear Circuits and Intelligent Information Processing, Chongqing 400715, China
[3]School of Optoelectronic Information, University of Electronic Science and Technology of Chengdu, Sichuan 611731, China

DOI:10.1109/JPHOT.2019.2945395

Manuscript received August 12, 2019; revised September 23, 2019; accepted September 30, 2019. Date of publication October 4, 2019; date of current version November 13, 2019. This work was supported by the Natural Science Foundation of Chongqing City under Grant Nos. cstc2016jcyjA0581, by the Postdoctoral Science Foundation of China under Grant Nos. 2016M590875, by the Fundamental Research Funds for the Central Universities under Grant XDJK2018B012. Corresponding author: Yi-Yuan Xie (e-mail: yyxie@swu.edu.cn).

Abstract: In this paper, tunable plasmon-induced transparency (PIT) is achieved in a novel and compact plasmonic system which consists of dual hexagonal resonators with rotatable rectangular bar embedded in resonators and a metal-insulator-metal (MIM) waveguide. The proposed structure is numerically investigated by finite-difference time-domain (FDTD) method. The numerical simulation results reveal that by rotating the embedded bar to different angles, PIT can realize in different wavelengths. Tunability in transparency peak wavelength, transmission, and optical delay are also obtained when the angle of embedded bars are changed. In addition, the influences of other structural parameters on transmission and optical delay are analyzed in detail. This proposed structure may provide a novel manipulation for tunable PIT and potentially be applied in highly integrated optical storage and switch devices.

Index Terms: Plasmon-induced transparency (PIT), rotatable bar, slow light, surface plasmon polaritons (SPPs).

1. Introduction

Plasmon-induced transparency (PIT), a kind of analogues electromagnetically induced transparency (EIT) in atomic systems, can generate a narrow transparency window within the absorption or transmission spectrum [1], [2]. Compared with the atomic EIT, PIT gets rid of the extreme requirement for experimental conditions and still has the corresponding characteristics, such as the abnormal dispersion which can remarkably slow down the group velocity of optical pulses [3]–[5]. Furthermore, PIT can be realized within the small footprint thanks to the capabilities provided by the surface plasmon polaritons (SPPs) to overcome classical diffraction limit and manipulate light in the nanoscale domain [6], [7]. So PIT has attracted a great deal of attention and various palsmonic structures have been proposed to achieve it such as metamaterials [8], graphene nanostrips [9], metal gratings [10], and metal-insulator-metal (MIM) waveguides [11]–[13]. Among these

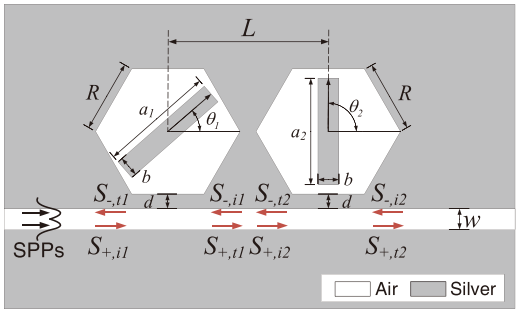

Fig. 1. The two dimensional schematic diagram of the proposed MIM waveguide PIT device.

different structures, MIM waveguides system is very suitable due to its advantages like strong light confinement, acceptable propagation length, and low bend loss [14], [15]. Additionally, plasmonic structure based on MIM waveguides is easily fabricated [16]. Therefore, a lot of PIT devices based on MIM waveguide have been introduced to realize momentous applications in sensors [17], logic gates [18], fillers [19], slow light devices [20], [21], and so on.

Nevertheless, MIM waveguide PIT devices still suffer from some unavoidable defects which limit the range of application. One of them is the fixed spectral response and operating frequency [22]. With the increase of integration requirements, many highly integrated photonic devices have to work at different frequencies. However, for most MIM waveguide PIT devices, the transparency windows are almost achieved at fixed wavelengths and they are barely modulated to different working frequencies [23]. Furthermore, in order to find more extensive and flexible applications of PIT device, other optical characteristics besides central wavelength such as transmission, bandwidth, and group index also should be able to be tuned [24]. In order to realize the tunability of PIT effect, the traditional scheme is to adjust the geometric dimensions of the structures directly [25]–[27]. It is widely agreed that the structural dimensions have important influence on device performance, but once the device is fabricated, it is difficult to change the structural dimensions [28], [29]. Consequently, it is imperative to find out other physical parameters except the geometric dimensions to be adjusted to obtain the tunable PIT phenomenon.

Motivated by the above fundamental studies, in this paper, the tunable PIT effect is obtained in a novel plasmonic structure which consists of dual side-coupled hexagonal resonators with rotatable embedded rectangular bar and a MIM straight waveguide. When the embedded bar rotates to different angle, the structural symmetry of hexagonal resonator is broken and the coupled situation between waveguide and resonator also changes. The finite-difference time-domain (FDTD) method with a perfectly matched layer (PML) absorbing boundary condition is used to numerically simulate the characteristics of proposed structure. Moreover, the effects of structural parameters on optical characteristics are also investigated in detail. This proposed compact chip-integrated PIT device will find many potential applications in the sensors, tunable switches, and slow light devices. This work also could offer a new concept to design the plasmonic devices.

2. Structure Model and Theoretical Analysis

The two dimensional schematic diagram of the proposed plasmonic structure in this paper is sketched in Fig. 1. Since hexagonal resonator has better resonant transmission contrast ratio and stronger coupling effect [30], two hexagonal resonators with a certain separation L are side coupled to a MIM straight waveguide whose width is constantly fixed to be $w = 50$ nm throughout this paper. Because the waveguide width is far smaller than the incident wavelength, there is only the fundamental transverse magnetic (TM) mode in the waveguide which can excite the SPPs waves. The side length of hexagonal resonators is R. $d = 20$ nm indicates the coupling distance between the boundary of resonators and waveguide. The long side lengths of two rectangular bars

embedded into the center of resonators are a_1 and a_2, and the short side lengths of them are both set to be b. Since these two rectangular bars are not stationary, θ_1 and θ_2 respectively donate the angles between the positive direction of x-axis and long side of rectangular bars. The insulator in MIM waveguides and hexagonal resonator is chosen to be air, whose refractive index is set as $n = 1$. The background metal is silver and its frequency-dependent complex relative permittivity can be characterized by the well-known Drude model: $\varepsilon_m(\omega) = \varepsilon_\infty - \omega_p^2/(\omega^2 + i\omega\gamma)$ [31]. Here ε_∞ represents the dielectric constant at the infinite frequency with the value of 3.7, $\omega_p = 9.1$ eV stands the bulk plasma frequency, $\gamma = 0.018$ eV is the electron collision frequency, and ω is the angular frequency of the incident wave [32]. In addition, other materials besides silver also can be used to fabricate the embedded bars.

As shown in Fig. 1, $S_{\pm,in}$ and $S_{\pm,tn}$ denote the amplitudes of incident and transmitted waves of the 1*st* and 2*nd* hexagonal resonator ($n = 1, 2$), respectively. The subscript $\pm$ represents two propagating directions. For the hexagonal resonator, the resonant wavelength λ_m should satisfy the phase condition [33]:

$$m \cdot 2\pi = \frac{2\pi}{\lambda_m}(6L)Re(N_{eff}) + \varphi \tag{1}$$

where N_{eff} is the effective index in hexagonal resonator and it is dependent on the refractive index of the dielectric material filled in hexagonal resonator, m is a positive integer corresponding to number of antimodes of the standing wave in the resonator, and φ is the total phase shift due to the corners and angles in the hexagonal resonator. Then the SPPs with resonant wavelength could be coupled into the resonator. The transmission characteristics can be investigated according to the couple-mode theory (CMT) [31]. The temporal evolution of normalized mode amplitude A_n of the resonator can be described as:

$$\begin{aligned}\frac{dA_n}{dt} = (-j\omega_n - k_{on} - k_{en})A_n + e^{j\varphi_n}\sqrt{k_{en}}S_{+,in} \\ + e^{j\varphi_n}\sqrt{k_{en}}S_{-,in}\end{aligned} \tag{2}$$

where ω_n represents the resonance frequency, k_{on} is the disintegration rate of the field due to the internal loss in resonator and k_{en} is the disintegration rate because of the power escape into the waveguide, and φ_n is the phase of coupling coefficient. $j = \sqrt{-1}$. If the time dependence is $e^{-j\omega t}$, the frequency of the input wave is ω and $dA_n/dt = -j\omega A_n$, we can deduce from equation (2) as follow at steady state:

$$A_n = \frac{e^{j\varphi_n}\sqrt{k_{en}}(s_{+,in} + s_{-,in})}{j(\omega_n - \omega) + k_{en} + k_{on}} \tag{3}$$

From energy conservation, the amplitude of the transmitted wave can be expressed as:

$$S_{+,tn} = S_{+,in} - e^{-j\varphi_n}\sqrt{k_{en}}A_n \tag{4a}$$

$$S_{-,tn} = S_{-,in} - e^{-j\varphi_n}\sqrt{k_{en}}A_n \tag{4b}$$

By solving equation (3) and (4) we can obtain the relation between incident and transmitted waves of the hexagonal resonator:

$$S_{-,in} = \frac{k_{en}}{j(\omega_n - \omega) + k_{on}}S_{+,in} + \frac{j(\omega_n - \omega) + k_{en} + k_{on}}{j(\omega_n - \omega) + k_{on}}S_{-,tn} \tag{5a}$$

$$S_{+,tn} = \frac{j(\omega_n - \omega) + k_{on} - k_{en}}{j(\omega_n - \omega) + k_{on}}S_{+,in} - \frac{k_{en}}{j(\omega_n - \omega) + k_{on}}S_{-,tn} \tag{5b}$$

Since the light is only launched from the left port ($S_{-,in} = 0$), the transmission t_n and reflection r_n of the single hexagonal resonator can be obtained as:

$$t_n = \frac{S_{+,tn}}{S_{+,in}} = \frac{j(\omega_n - \omega) + k_{on}}{j(\omega_n - \omega) + k_{on} + k_{en}} \tag{6a}$$

$$r_n = \frac{S_{-,tn}}{S_{+,in}} = -\frac{k_{en}}{j(\omega_n - \omega) + k_{on} + k_{en}} \tag{6b}$$

Furthermore, the following matrix can be used to express the incident and transmitted waves of the resonator.

$$\begin{bmatrix} S_{-,in} \\ S_{+,tn} \end{bmatrix} = \begin{bmatrix} -\frac{r_n}{t_n} & \frac{1}{t_n} \\ 1 + \frac{r_n}{t_n} & \frac{r_n}{t_n} \end{bmatrix} \begin{bmatrix} S_{+,in} \\ S_{-,tn} \end{bmatrix} \tag{7}$$

For the propagation waves in the bus waveguide, there is a relationship which they should satisfy as follow:

$$S_{-,i1} = S_{-,t2} e^{j\phi} \tag{8a}$$

$$S_{+,i2} = S_{+,t1} e^{j\phi} \tag{8b}$$

Here ϕ is the phase difference between two hexagonal resonators. Thus, the incident and output waves of the whole plasmonic structure can be obtained as:

$$\begin{bmatrix} S_{-,i2} \\ S_{+,t2} \end{bmatrix} = \begin{bmatrix} -\frac{r_2}{t_2} & \frac{1}{t_2} \\ 1 + \frac{r_2}{t_2} & \frac{r_2}{t_2} \end{bmatrix} \begin{bmatrix} 0 & e^{j\phi} \\ e^{-j\phi} & 0 \end{bmatrix} \begin{bmatrix} -\frac{r_1}{t_1} & \frac{1}{t_1} \\ 1 + \frac{r_1}{t_1} & \frac{r_1}{t_1} \end{bmatrix} \begin{bmatrix} S_{+,i1} \\ S_{-,t1} \end{bmatrix} \tag{9}$$

Since the incident light is only inputted from the left port of waveguide, the transmission efficiency T at the right port can be derived as:

$$T = \left| \frac{S_{+,t2}}{S_{+,i1}} \right|^2 = \left| \frac{t_1 t_2}{1 - r_1 r_2 e^{j2\phi}} \right|^2 = \left(\frac{|t_1 t_2|}{1 - |r_1 r_2|} \right)^2 \frac{1}{1 + 4 \left(\frac{\sqrt{|r_1 r_2|}}{1 - |r_1 r_2|} \right)^2 \sin^2 \frac{\vartheta}{2}} \tag{10}$$

According to the previous research, the transmission characteristic of a Fabry Perot resonator with two frequency-dependent mirrors can be calculated by this equation [31]. Here, $\vartheta = Arg[r_1 r_2 \exp(j2\phi)]$ is the round-trip phase in the Fabry Perot resonator which is related to the certain separation L. As L is designed specially to satisfy the condition that ϑ is close to the multiple of 2π, T has the maximum $T_{max} = [|t_1 t_2|/(1 - |r_1 r_2|)]^2$ and a transparency window which indicates the PIT Phenomenon appears in the spectrum. Since $t_{1,2}$ and $r_{1,2}$ are all relevant to the resonant wavelengths, the maximum transmission T_{max} is depends on the resonance frequencies of two resonators [31]. Besides, the central wavelength of transparency peak is another parameter which is influenced by resonant wavelengths [34]. So when the resonance frequencies of two resonators changes, the transmission and the central wavelength of transparency peak are all varied. Based on equation (1), we know that the resonant wavelength of hexagonal resonator is related to many factors such as the effective index, the side length, and the total phase shift in the hexagonal resonator. The conventional method is adjusting the side length of resonator, it is inconvenient since once the optical device is fabricated, it is difficult to change the structural dimensions. In the proposed plasmonic structure, since the rotatable rectangular insertion is embedded into the center of hexagonal resonator to introduce the structural asymmetry, the total phase shift will change with the rotation of the insertion. So the adjustment of resonant wavelength of hexagonal resonator can be realized by rotating the embedded rectangular bar. Therefore, this plasmonic structure can achieve the tunable PIT by rotating the embedded bar in the resonator. Nowadays, in many micro electro-mechanical-system (MOEMS) and micro-opto-electro-mechanical systems (MOEMS) like

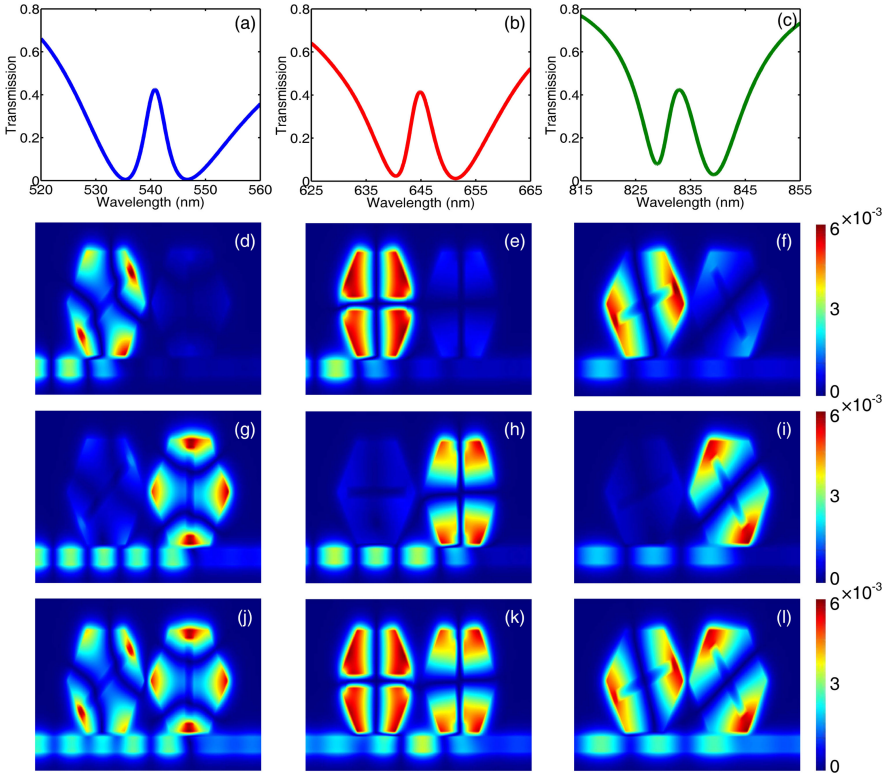

Fig. 2. (a) Transmission spectrum of transparency window peak1, (d), (g), and (j) field distributions of *Hz* at 535.6 nm, 546.6 nm, and 540.8 nm with rotating angle $\theta_1 = 40^\circ$ and $\theta_2 = 90^\circ$. (b) Transmission spectrum of transparency window peak2, (e), (h), and (k) field distributions of *Hz* at 640.4 nm, 651.3 nm, and 644.9 nm with rotating angle $\theta_1 = 0^\circ$ and $\theta_2 = 90^\circ$. (c) Transmission spectrum of transparency window peak3, (f), (i), and (l) field distributions of *Hz* at 828.9 nm, 839.2 nm, and 832.9 nm with rotating angle $\theta_1 = 20^\circ$ and $\theta_2 = 125^\circ$.

gyroscope and micromirror, the rotation can be flexibly realized [35], [36]. Moreover, nanomechanical rotors are of great technological interest to achieve the rotation of nanorod or bar in the micro and nanoscale. For instance, an optically trapped silicon nanorod set into rotation at MHz frequencies was demonstrated to work as an ultra-stable nanomechanical rotor [37]. An optical rotor based on a nano-scale Si pn junction wire could rotate with acceleration under the green-light illumination [38]. The single-electron tunneling effect also can be used to dynamically drive the nanorod to rotate around the axis in the middle of rod [39]. Especially, an optical rotor inside a silica substrate which is often chosen to be the substrate of plasmonic structure has been fabricated using femtosecond laser-assisted etching and it can spun under laser trapping with rotation speed controlled by the trapping laser power [40]. So the rotation of embedded bar is feasible with the support of these methods like proposed in Ref. [40].

3. Simulation Results and Analysis

3.1 Transmission Characteristic and Slow Light Effect

The transmission properties of SPP wave in the proposed structure is numerically investigated using the finite-difference time-domain (FDTD) method. The side lengths of two hexagonal resonators are $R = 200$ nm. The certain separation L between two resonators is 440 nm. The long side lengths of two rectangular bars embedded in resonators are $a_1 = 320$ nm and $a_2 = 295$ nm, respectively. The short side lengths are $b = 50$ nm. In the FDTD simulations, the absorbing boundary condition is set to be a perfectly matched layer (PML). In Fig. 2(a), the transparency window appears in

the simulated transmission spectrum when the rotating angle θ_1 is 40° and θ_2 is 90°, a narrow peak appears at 540.8 nm, meanwhile, there are two transmission dips locate at the wavelength 535.6 nm and 546.6 nm. It is the typical feature of PIT phenomenon. The field distribution of $|H_z|$ in the plasmonic structure at two transmission dips and transparency peak are shown in Fig. 2(d), Fig. 2(g) and Fig. 2(j), respectively. It can be found from the field distributions that when the wavelength of incident wave is 535.6 nm or 546.6 nm, the local resonance in the individual hexagonal resonator is excited and the incident wave is prohibited to transmit along the MIM waveguide to the through port due to the destructive interference between the incident wave and wave escaped from the hexagonal resonator. As for the wavelength of transparency peak 540.8 nm, the field distribution shown in Fig. 2(j) depicts that two resonators form the Fabry-Perot oscillation in the bus waveguide, and the incident wave can pass through the waveguide and output from the right port since the waves through two mirrors generate the destructive interference, so the previous destructive interference between the incident wave and escaped wave from hexagonal resonator is not exist. It is consistent with the transmission spectrum in Fig 2(a).

When the rectangular bar in the left hexagonal resonator is rotated to $\theta_1 = 0°$ and the rotating angle θ_2 is kept as 90°, a narrow transmission peak occurs at wavelength 644.9 nm due to the PIT phenomenon. Fig. 2(e), Fig. 2(h) and Fig. 2(k) are the field distributions of $|H_z|$ at the wavelengths of transmission dips and peak, they prove that it is similar to the situation when the rotating angle θ_1 is 40° and θ_2 is 90°. Analogously, a obvious narrow transmission peak occurs at the center wavelength 832.9 nm between two transmission dips when the rotating angle θ_1 is 20° and θ_2 is 125°. The local resonances in two hexagonal resonators are excited at the wavelength of transmission dips 828.9 nm and 839.2 nm. Most energy of the incident wave is coupled into the resonator and there is a dip at the resonance wavelength in transmission spectrum. As the same, at the wavelength 832.9 nm the destructive interference between the incident wave and escaped wave from hexagonal resonator disappears, so the incident wave can output from the right port and there is the transparency window shown in the transmission spectrum.

An important usage of PIT phenomenon is to support the slow light propagation in nanoscale. Based on the above simulated results, we know that the proposed plasmonic structure can achieve tunable PIT phenomenon by rotating the embedded rectangular bars to different angles. Therefore, it also has the capability to achieve slow light. Generally, the group index n_g is an effective parameter used to described the slow light and it can be expressed as

$$n_g = \frac{c}{v_g} = \frac{c}{D}\tau_g = \frac{c}{D}\frac{d\psi(\omega)}{d\omega} \tag{11}$$

Here v_g and τ_g are the group velocity and optical delay time, respectively. D is the length of the plasmonic structure. $\psi(\omega)$ is the transmission phase shift and it can be calculated by $\psi(\omega) =$ angular($\frac{S_{+,t2}}{S_{+,i1}}$). The slow light performance is numerically investigated in the proposed plasmonic structure with $R = 200$ nm, $L = 440$ nm, $d = 20$ nm, $b = 50$ nm, $a_1 = 320$ nm, and $a_2 = 295$ nm. Fig. 3(a) is the phase shift in the through port when rotating angle $\theta_1 = 40°$ and $\theta_2 = 90°$. It can be obtained that the phase slope is negative and the steepest at the center wavelength of the transparency window. According to equation (11), we can get that there is the large optical delay during the transparency window, and the maximum delay time is about 0.07 ps at the narrow peak wavelength as shown in Fig. 3(d). The corresponding group index depicted in Fig. 3(g) is over 17 in the center wavelength due to the strong dispersion in the transparency window. The rest in Fig. 3 show that when the rotating angle $\theta_1 = 0°$ and $\theta_2 = 90°$ or θ_1 is 20° and θ_2 is 125°, the proposed structure can realize the slow light effect with 0.75 ps optical delay time in other wavelengths.

3.2 Influence of the Rotating Angles

Based on the theoretical analysis and above numerical simulations, it is certain that the rotating angles of the embedded rectangular bar have important impact on the PIT phenomenon, namely the rotating angles θ_1 and θ_2 are the key factor to realize the tunable PIT phenomenon at different wavelengths in the proposed structure. Therefore, in order to verify the feasibility of achieving tunable

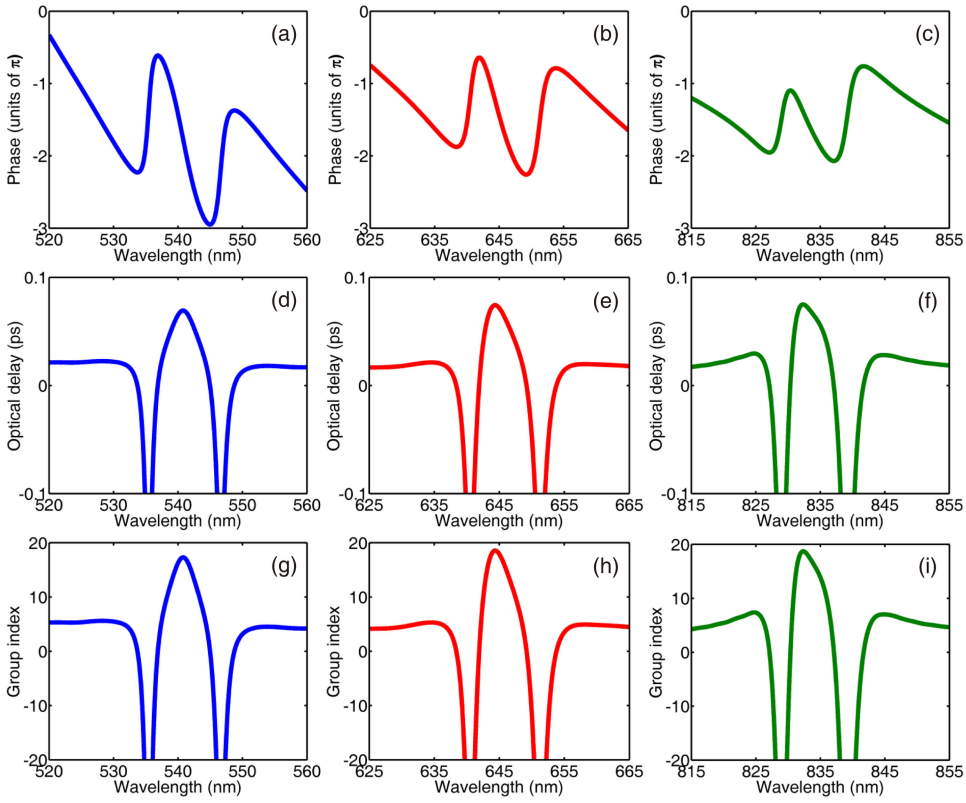

Fig. 3. (a) Transmission phase shift, (d) optical delay time, and (g) group index in the proposed structure with rotating angle $\theta_1 = 40^\circ$ and $\theta_2 = 90^\circ$. (b) Transmission phase shift, (e) optical delay time, and (h) group index in the proposed structure with rotating angle $\theta_1 = 0^\circ$ and $\theta_2 = 90^\circ$. (c) Transmission phase shift, (f) optical delay time, and (i) group index in the proposed structure with rotating angle $\theta_1 = 20^\circ$ and $\theta_2 = 125^\circ$.

PIT phenomenon in different wavelength range through rotating the inserted bar, the influence of the rotating angles on transmission characteristics and slow light performance is studied by FDTD simulations. Fig. 4(a), 4(b), and 4(c) show the relationship between rotating angle θ_1 and resonance wavelength, transmission, and optical delay respectively, when θ_1 is increased from 30° to 50° in steps of 2.5° and θ_2 is kept as 90°. It can be observed that the resonance wavelength red-shifts and transmission characteristic rises with the increase of θ_1, however, the optical delay time is decreasing. The effect of rotating angle θ_2 on these parameters is also investigated and shown in Fig. 4(d), 4(e), and 4(f). In this time, rotating angle θ_1 is set as 40° and rotating angle θ_2 is increased from 80° to 100°.

As shown in Fig. 5, both the rotating angles θ_1 and θ_2 have important influence on the PIT effect when the transparency window is adjusted to appear at wavelength 644.9 nm. When θ_1 increases from -10° to 0°, the resonance wavelength shifts to small wavelength but redshifts to large wavelength as θ_1 keeps increasing. Transmission characteristic firstly decreases and then increases to the maximum as θ_1 increases to 0°. However, when θ_1 keeps increasing to 10°, the transmission characteristic firstly decreases to 2.396% and then increases to 39.23% again. The optical delay has the similar trend with the rotation of rectangular bar. Then, the resonance wavelength, transmission, and optical delay as functions of the rotating angle θ_2 with θ_1 is 0° are shown in Figs. 5(d)–5(f). They all change with the rotation of embedded bar and when θ_2 is 90°, the resonance wavelength and transmission both reach the maximum. As for the optical delay time, its value is 0.072 ps.

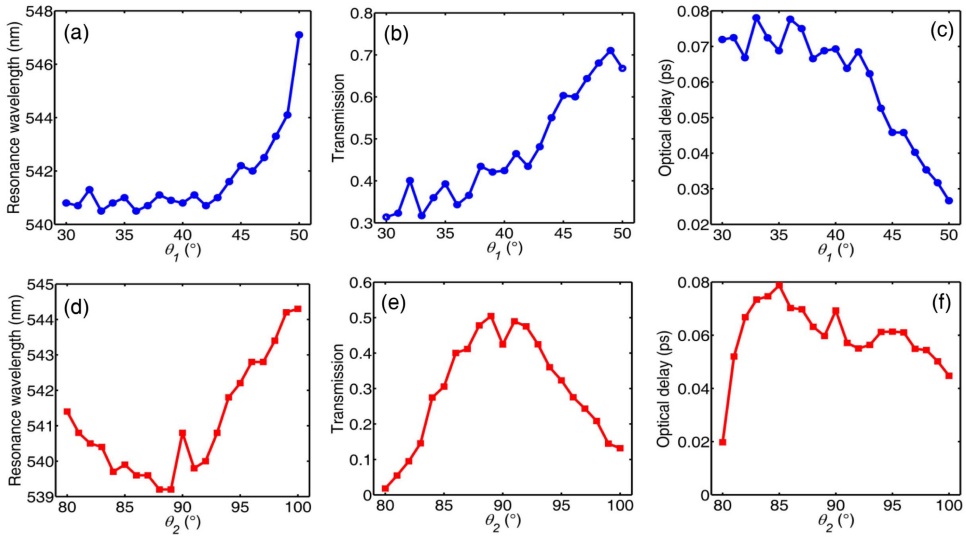

Fig. 4. (a) Resonance wavelength, (b) transmission of peak1, and (c) optical delay time versus the rotating angle θ_1 during 30° to 50°. (d) Resonance wavelength, (e) transmission of peak1, and (f) optical delay time versus the rotating angle θ_2 during 80° to 100°.

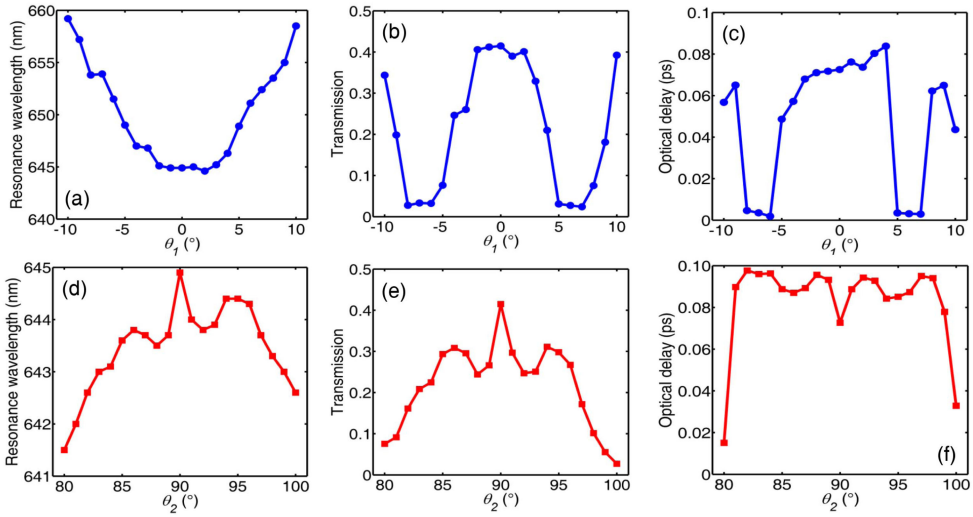

Fig. 5. (a) Resonance wavelength, (b) transmission of peak2, and (c) optical delay time in different rotating angle θ_1 during $-10°$ to 10°. (d) Resonance wavelength, (e) transmission of peak2, and (f) optical delay time in different rotating angle θ_2 during 80° to 100°.

Finally, the relationships between the performances used to describe PIT phenomenon and rotating angles when the initial value of rotating angle θ_1 is 20° and θ_2 is 125° are investigated and shown in Fig. 6. Whether θ_1 or θ_2 is fixed and the other insertion is rotated, the resonance wavelength of the proposed structure is blue-shifted to lower wavelength. Meanwhile, the transmission is increasing with the rotation of the rectangular bar in the left hexagonal resonator, and it reaches the maximum when θ_1 is 20°. As the rectangular bar continues to rotate, the transmission is gradually reduced. The optical delay decreases as the rotation angle of embedded bar increases. And when the rectangular bar in left hexagonal resonator is fixed, rotating the rectangular bar which is embedded in the right hexagonal resonator will lead to the variations of the PIT phenomenon. Both

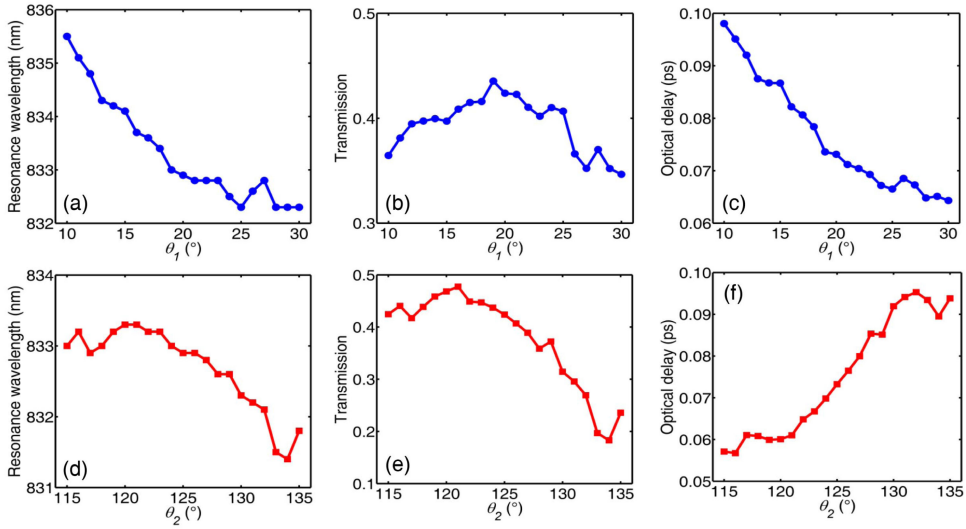

Fig. 6. (a) Resonance wavelength, (b) transmission of peak3, and (c) optical delay time in different rotating angle θ_1 during 10° to 30°. (d) Resonance wavelength, (e) transmission of peak3, and (f) optical delay time in different rotating angle θ_2 during 115° to 135°.

the resonance wavelength and transmission decrease as the rotating angle θ_2 increases. Contrary to the case when the rectangular bar in left resonator is rotated, as the rotation angle θ_2 increases, the optical delay also increases. Hence, the tunable PIT phenomenon can be realized by adjusting the angle θ_1 and θ_2 of two inserted bar in the center of hexagonal resonators through rotating them.

3.3 Influence of Structural Geometrical Dimensions

It must be acknowledged that geometrical dimensions of structure still has a negligible effect on the performance of the device. Therefore, the parametric study of the proposed structure is also critical to optimizing device performance. Firstly, in order to investigate the effect of side length of hexagonal resonator, R is increased from 195 nm to 210 nm in 5-nm steps, the other structural parameters are kept as $L = 440$ nm, $d = 20$ nm, $b = 50$ nm, $a_1 = 320$ nm, and $a_2 = 295$ nm. Fig. 7 is the simulated transmission spectra and optical delay time for different side length R when the rotating angles are $\theta_1 = 40°$ and $\theta_2 = 90°$, $\theta_1 = 0°$ and $\theta_2 = 90°$, $\theta_1 = 20°$ and $\theta_2 = 125°$ respectively. All wavelengths of the transparency windows exhibit red-shifts with the increase of side length and the transmissions of the narrow peaks decrease. In addition, increasing the side length also affects the optical delay time. For transparency windows of different wavelengths, the variation of optical delay caused by the change of side length is different from each other. There is difference between the change trends of optical delay time and transmission. Therefore, a trade-off between the peak transmission and optical delay time must to be considered.

According to the theoretical analysis, the round-trip phase of the Fabry-Perot resonator has important effect on transmission and it is controlled by the optical path difference which is relevant to the certain separation L in this proposed structure. Fig. 8(a) shows the relationship between the certain separation L and transmission of all transparency windows at different wavelengths where Peak1, peak2, and peak3 represent the narrow transparency peak when rotating angles are $\theta_1 = 40°$ and $\theta_2 = 90°$, $\theta_1 = 0°$ and $\theta_2 = 90°$, $\theta_1 = 20°$ and $\theta_2 = 125°$ respectively. The variation trends of transmission of peak1 and peak2 are similar to some extent and the same goes for optical delay as shown in Fig. 8(b). They both reach the maximum when the certain separation L is 440 nm. As for the peak3 when the rotating angle $\theta_1 = 20°$ and $\theta_2 = 125°$, both transmission and optical delay increase as the certain separation L increases.

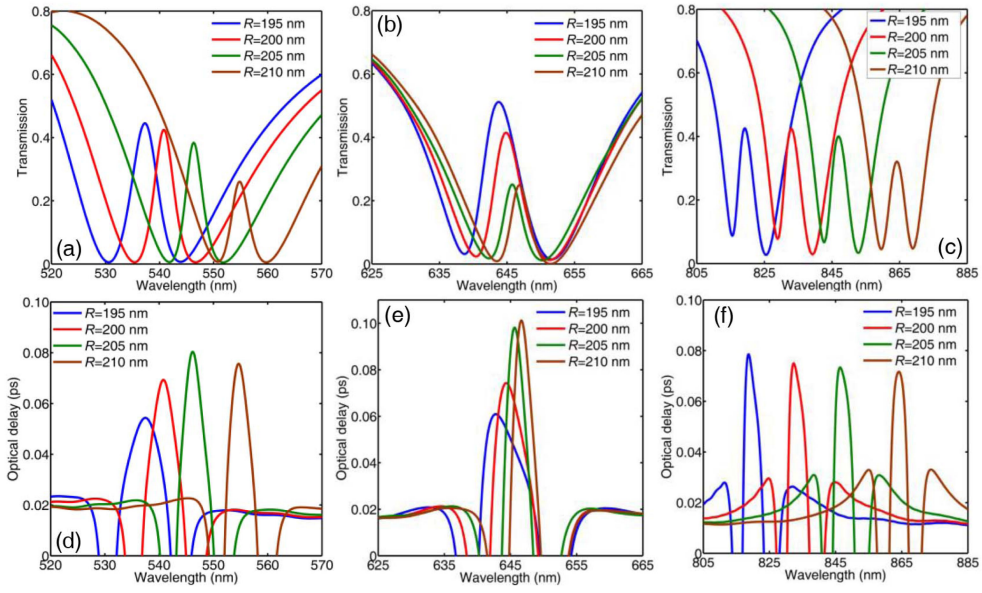

Fig. 7. Transmission spectra and optical delay time change as side length of hexagonal resonator R. The rotating angles are set as $\theta_1 = 40^\circ$ and $\theta_2 = 90^\circ$ (a) (d), $\theta_1 = 0^\circ$ and $\theta_2 = 90^\circ$ (b) (e), $\theta_1 = 20^\circ$ and $\theta_2 = 125^\circ$ (c) (f).

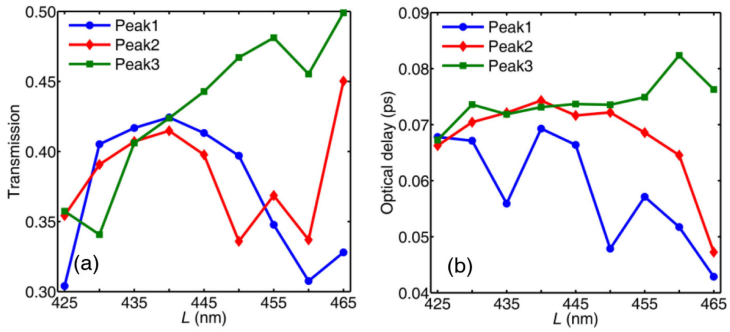

Fig. 8. (a) Transmission and (b) optical delay time as functions of the certain separation L of peak1 (blue line), peak2 (red line), and peak3 (green line).

Successively, to investigate how the structural parameters of two embedded rectangular bar affect the transmission and optical delay time of the proposed device, the long side length a_1 is increased from 280 nm to 330 nm in 5-nm steps while the long side length a_2 is fixed as 295 nm. As shown in Fig. 9(a) and 9(d), the long side length a_1 has great influence on the transmission and optical delay of peak1 and peak2, but the transmission and optical delay of peak3 are less varied with the changes of long side length a_1. Then, the long side length a_2 is increased from 280 nm to 330 nm while the long side length a_1 is fixed as 320 nm. Fig. 9(b) shows the relationships between the transmission of all narrow peak in transparency window and the long side length a_2. It is exactly the opposite of the influence of long side length a_1 on transmissions, with the increase of a_2, the transmission of peak1 decreases when the transmission of peak2 increases. Similarly, the transmission of peak3 is less affected and it only rises from 40.36% to 51.88%. Fig. 9(e) shows the change of optical delay with the long side length a_2. The delay time of peak1 increases and the delay time of peak2 decreases as long side length a_2 increases. The situation of change of peak3 delay time is similar to the transmission and it is less affected. Furthermore, the influence of the

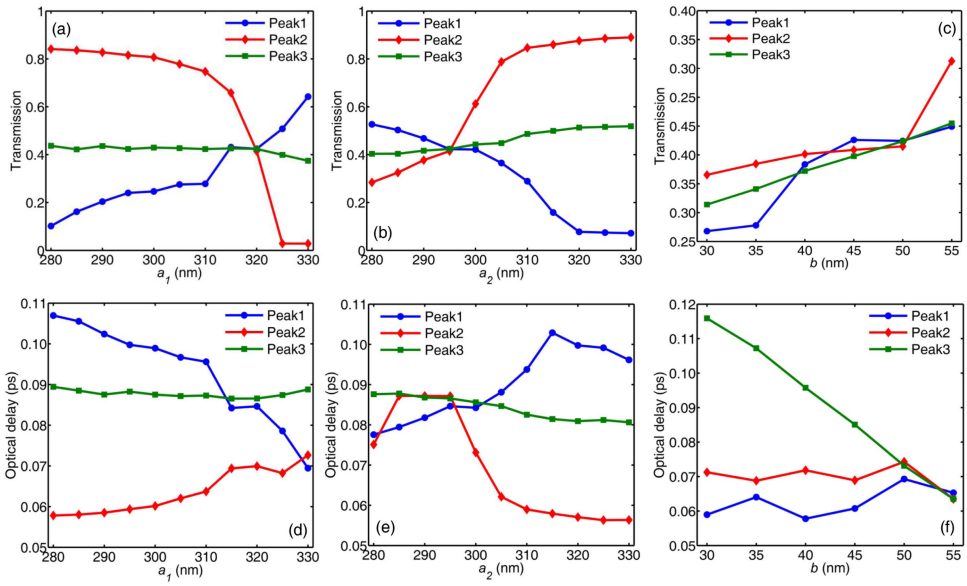

Fig. 9. Transmission of transparency peaks as functions of (a) long side length a_1, (b) long side length of a_2, and (c) short side length b. Optical delay time of transparency peaks as functions of (d) long side length a_1, (e) long side length of a_2, and (f) short side length b.

short side length b on transmission and delay time of all peaks is also studied and shown in Fig. 9(c) and 9(f). It together with previous research on other structural parameters provide simulated results to help the optimization of the proposed device.

4. Conclusion

In summary, the tunable plasmon-induced transparency is investigated in a novel and compact plasmonic system which is constructed by a MIM waveguide with dual hexagonal resonators where rotatable rectangular silver bar is embedded. The FDTD simulation results illustrate that by rotating the embedded bar to different angles, the structural symmetry of resonator is broken and the transparency window, the typical representation of PIT phenomenon, can be realized in different wavelength ranges. The peak wavelength, transmission, and optical delay time will change with the rotation of embedded rectangular bars. Moreover, the other structural parameters such as side length of the resonator, certain separation between two resonators, long and short side lengths of the rectangular bars also have influence on the transmission characteristics and optical delay time. This plasmonic device may provide a novel method for obtaining the tunable plasmon-induced transparency and have great potential application in highly integrated optical circuits for optical storage and switching.

Acknowledgment

The authors wish to thank the anonymous reviewers for their valuable suggestions.

References

[1] S. Zhang, D. A. Genov, Y. Wang, M. Liu, and X. Zhang, "Plasmon-induced transparency in metamaterials," *Phys. Rev. Lett.*, vol. 101, no. 4, Jul. 2008, Art. no. 047401.
[2] N. Liu *et al.*, "Plasmonic analogue of electromagnetically induced transparency at the drude damping limit," *Nat. Mater.*, vol. 8, no. 9, pp. 758–762, Sep. 2009.

[3] R. D. Kekatpure, E. S. Barnard, W. Cai, and M. L. Brongersma, "Phase-coupled plasmon-induced transparency," *Phys. Rev. Lett.*, vol. 104, no. 24, Jun. 2010, Art. no. 243902.
[4] G. Yao, F. Ling, J. Yue, Q. Luo, and J. Yao, "Dynamically tunable graphene plasmon-induced transparency in the terahertz region," *J. Lightw. Technol.*, vol. 34, no. 16, pp. 3937–3942, Aug. 2016.
[5] L. He, T. Wang, Y. Gao, C. Cao, and C. Wang, "Discerning electromagnetically induced transparency from autler-townes splitting in plasmonic waveguide and coupled resonators system," *Opt. Exp.*, vol. 23, no. 18, pp. 23 817–23 826, Sep. 2015.
[6] D. K. Gramotnev and S. I. Bozhevolnyi, "Plasmonics beyond the diffraction limit," *Nat. Photon.*, vol. 4, no. 2, pp. 83–91, Jan. 2010.
[7] W. L. Barnes, A. Dereux, and T. W. Ebbesen, "Surface plasmon subwavelength optics," *Nature*, vol. 424, no. 6950, pp. 824–830, Aug. 2003.
[8] M. Miyata, J. Hirohata, Y. Nagasaki, and J. Takahara, "Multi-spectral plasmon induced transparency via in-plane dipole and dual-quadrupole coupling," *Opt. Exp.*, vol. 22, no. 10, pp. 11 399–11 406, May 2014.
[9] X. Zhao, L. Zhu, C. Yuan, and J. Yao, "Tunable plasmon-induced transparency in a grating-coupled double-layer graphene hybrid system at far-infrared frequencies," *Opt. Lett.*, vol. 41, no. 23, pp. 5470–5473, Dec. 2016.
[10] Z. Chai, X. Hu, Y. Zhu, F. Zhang, H. Yang, and Q. Gong, "Low-power and ultrafast all-optical tunable plasmon-induced transparency in plasmonic nanostructures," *Appl. Phys. Lett.*, vol. 102, no. 20, 2013, Art. no. 201119.
[11] Z. Han and S. I. Bozhevolnyi, "Plasmon-induced transparency with detuned ultracompact fabry-perot resonators in integrated plasmonic devices," *Opt. Exp.*, vol. 19, no. 4, pp. 3251–3257, Feb. 2011.
[12] Q. Lu *et al.*, "Plasmon-induced transparency and high-performance slow light in a plasmonic single-mode and two-mode resonators coupled system," *J. Lightw. Technol.*, vol. 35, no. 9, pp. 1710–1717, May 2017.
[13] X. Han, T. Wang, X. Li, B. Liu, Y. He, and J. Tang, "Dynamically tunable slow light based on plasmon induced transparency in disk resonators coupled mdm waveguide system," *J. Phys. D: Appl. Phys.*, vol. 48, no. 23, May 2015, Art. no. 235102.
[14] Y. Zhu, X. Hu, H. Yang, and Q. Gong, "On-chip plasmon-induced transparency based on plasmonic coupled nanocavities," *Sci. Rep.*, vol. 4, p. 3752, Jan. 2014.
[15] M. R. Rakhshani and M. A. Mansouri-Birjandi, "High sensitivity plasmonic refractive index sensing and its application for human blood group identification," *Sens. Actuators B*, vol. 249, pp. 168–176, Apr. 2017.
[16] L. Xu, S. Wang, and L. Wu, "Refractive index sensing based on plasmonic waveguide side coupled with bilaterally located double cavities," *IEEE Trans. Nanotechnol.*, vol. 13, no. 5, pp. 875–880, Sep. 2014.
[17] B. Li, H. Li, L. Zeng, S. Zhan, Z. He, Z. Chen, and H. Xu, "High-sensitivity sensing based on plasmon-induced transparency," *IEEE Photon. J.*, vol. 7, no. 5, Oct. 2015, Art. no. 4801207.
[18] Y. Ye, Y. Xie, Y. Liu, S. Wang, J. Zhang, and Y. Liu, "Design of a compact logic device based on plasmon-induced transparency," *IEEE Photon. Technol. Lett.*, vol. 29, no. 8, pp. 647–650, Apr. 2017.
[19] Z. He and Z. Zhou, "Theoretically analyze the tunable wide band-stop filtering in plasmonic waveguide coupled with fixed height to length stubs," *IEEE Photon. J.*, vol. 10, no. 6, Dec. 2018, Art. no. 4801208.
[20] Y. Huang, C. Min, P. Dastmalchi, and G. Veronis, "Slow-light enhanced subwavelength plasmonic waveguide refractive index sensors," *Opt. Exp.*, vol. 23, no. 11, pp. 14 922–14 936, May 2015.
[21] H. Li, L. Wang, and X. Zhai, "Plasmonically induced absorption and transparency based on MIM waveguides with concentric nanorings," *IEEE Photon. Technol. Lett.*, vol. 28, no. 13, pp. 1454–1457, Jul. 2016.
[22] B. Zhang *et al.*, "Absorption and slow-light analysis based on tunable plasmon-induced transparency in patterned graphene metamaterial," *Opt. Exp.*, vol. 27, no. 3, pp. 3598–3608, Feb. 2019.
[23] P. Qiu *et al.*, "Dynamically tunable plasmon-induced transparency in on-chip graphene-based asymmetrical nanocavity-coupled waveguide system," *Nanoscale Res. Lett.*, vol. 12, no. 1, p. 374, Feb. 2017.
[24] T. Zhang *et al.*, "Tunable plasmon induced transparency in a metallodielectric grating coupled with graphene metamaterials," *J. Lightw. Technol.*, vol. 35, no. 23, pp. 5142–5149, Dec. 2017.
[25] J. Wang, Y. Niu, D. Liu, Z.-D. Hu, T. Sang, and S. Gao, "Tunable plasmon-induced transparency effect in mim side-coupled isosceles trapezoid cavities system," *Plasmonics*, vol. 13, no. 2, pp. 609–616, Apr. 2018.
[26] Z. Chen, X. Song, R. Jiao, G. Duan, L. Wang, and L. Yu, "Tunable electromagnetically induced transparency in plasmonic system and its application in nanosensor and spectral splitting," *IEEE Photon. J.*, vol. 7, no. 6, Dec. 2015, Art. no. 4801408.
[27] D. Liu *et al.*, "Plasmon-induced transparency and refractive index sensing based on a trapezoid cavity coupled with a hexagonal resonator," *Plasmonics*, vol. 14, no. 3, pp. 663–671, Sep. 2019.
[28] X. Han, T. Wang, X. Li, S. Xiao, and Y. Zhu, "Dynamically tunable plasmon induced transparency in a graphene-based nanoribbon waveguide coupled with graphene rectangular resonators structure on sapphire substrate," *Opt. Exp.*, vol. 23, no. 25, pp. 31 945–31 955, Dec. 2015.
[29] H. Xu, H. Li, Z. He, Z. Chen, M. Zheng, and M. Zhao, "Dual tunable plasmon-induced transparency based on silicon–air grating coupled graphene structure in terahertz metamaterial," *Opt. Exp.*, vol. 25, no. 17, pp. 20 780–20 790, Aug. 2017.
[30] Y. Xie, Y. Ye, Y. Liu, S. Wang, J. Zhang, and Y. Liu, "Synchronous slow and fast light based on plasmon-induced transparency and absorption in dual hexagonal ring resonators," *IEEE Trans. Nanotechnol.*, vol. 17, no. 3, pp. 552–558, May 2018.
[31] H. Lu, X. Liu, and D. Mao, "Plasmonic analog of electromagnetically induced transparency in multi-nanoresonator-coupled waveguide systems," *Phys. Rev. A*, vol. 85, no. 5, p. 053803, May 2012.
[32] Z. Han, E. Forsberg, and S. He, "Surface plasmon bragg gratings formed in metal-insulator-metal waveguides," *IEEE Photon. Technol. Lett.*, vol. 19, no. 2, pp. 91–93, Jan. 2007.
[33] Y. Xie, Y. Huang, W. Zhao, W. Xu, and C. He, "A novel plasmonic sensor based on metal–insulator–metal waveguide with side-coupled hexagonal cavity," *IEEE Photon. J.*, vol. 7, no. 2, Apr. 2015, Art. no. 4800612.
[34] X. Yang, M. Yu, D.-L. Kwong, and C. W. Wong, "All-optical analog to electromagnetically induced transparency in multiple coupled photonic crystal cavities," *Phys. Rev. Lett.*, vol. 102, no. 17, May 2009, Art. no. 173902.

[35] X. Shen, L. Zhao, and D. Xia, "Esearch on the disc sensitive structure of a Micro Optoelectromechanical System (MOEMS) resonator gyroscope," *Micromachines*, vol. 10, no. 4, p. 264, Apr. 2019.
[36] M. Pallapa and J. Yeow, "Design, fabrication and testing of a polymer composite based hard-magnetic mirror for biomedical scanning applications," *J. Electrochem. Soc.*, vol. 161, no. 2, pp. B3006–b3013, Oct. 2013.
[37] S. Kuhn *et al.*, "Optically driven ultra-stable nanomechanical rotor," *Nat. Commun.*, vol. 8, no. 1, p. 1670, Nov. 2017.
[38] Y. Omura, "Potential of nano-scale optical rotor based on a pn-junction wire," in *Proc. Silicon Nanoelectronics Workshop*, Jun. 2019, pp. 1–2.
[39] A. Croy and A. Eisfeld, "Dynamics of a nanoscale rotor driven by single-electron tunneling," *Europhys. Lett.*, vol. 98, Jun. 2012, Art. no. 68004.
[40] S. Matsuo *et al.*, "Laser microfabrication and rotation of ship-in-a-bottle optical rotators," *Appl. Phys. Lett.*, vol. 93, no. 5, Aug. 2008, Art. no. 051107.